Proceedings World Geothermal Congress 2026
Calgary, Canada, June 8 – 11, 2026

Reducing Drilling Costs and Maximizing Energy Extraction in a Geothermal Well with Advanced Temperature-Pressure Management Controllers

Yifan Zhang[1*], Xu Duan[1], Santiago Callerio[1], Pradeepkumar Ashok[1], Dongmei Chen[1], Eric van Oort[1], Chuck Wright[2], and Guizhong Chen[2*]

The University of Texas at Austin[1], NOV Springett Technology Center[2]

yfzhang@utexas.edu, gary.chen@nov.com

Keywords: geothermal test well, bottomhole circulating temperature (BHCT) control, managed temperature drilling (MTD), managed pressure drilling (MPD).

ABSTRACT

Effective management of downhole temperature and pressure is essential for both drilling and production of geothermal wells to ensure well integrity, enhance energy extraction, reduce operational risks, and improve overall project economics. This study presents a novel real-time control framework for coupled temperature-pressure management in geothermal and high-pressure-high-temperature (HPHT) wells. The proposed solution is demonstrated through thermal-hydraulics simulations of a 11,503 ft well with a static, undisturbed bottomhole temperature of approximately 275 °F. Three control strategies, proportional-integral-derivative (PID), linear-quadratic-integral (LQI), and iterative linear-quadratic-regulator (iLQR), were developed from a control-oriented physics-based model and evaluated for varying nonlinear well control operations. Mud flow rate, inlet mud temperature, and choke opening were used as the primary control inputs. Simulation results demonstrate that the integrated managed-pressure-managed-temperature drilling (MPD-MTD) framework can achieve rapid bottomhole circulation temperature (BHCT) stabilization while maintaining bottomhole pressure (BHP) fluctuations to within 30 psi for the subject well. Compared to conventional well temperature and pressure control methods, the proposed approach provides a faster response, higher accuracy, improved efficiency, and enhanced robustness.

1 INTRODUCTION

Geothermal energy provides a clean, renewable, and continuously available power source with the potential for large-scale, long-term energy security. Emerging concepts such as superhot rock geothermal, targeting ultra-deep formations exceeding 750+ °F in-situ temperatures, could greatly increase the power density and efficiency of geothermal wells, positioning geothermal as a highly promising pathway for sustainable, high-output energy generation.

As geothermal and high-pressure-high-temperature (HPHT) wells are drilled deeper and larger diameters, drilling and completion become increasingly challenging and costly due to extreme downhole temperatures and pressures. Effective management of these conditions is critical for maintaining wellbore integrity, protecting equipment, and ensuring stable energy extraction. However, traditional well temperature and pressure control strategies rely heavily on manual design and control operation, making them heavily dependent on the experience of drilling engineers and drillers out in the field, are often insufficient for rapid suppression of unexpected thermal-pressure shocks.

Advances in high-fidelity thermal-hydraulics modeling, distributed well telemetry, rig digitalization, and advanced rig equipment enable a more systematic approach to automatically predict and regulate downhole pressures and temperatures. These developments form the foundation of managed-pressure-managed-temperature drilling (MPD-MTD), which aims to minimize bottomhole pressure (BHP) fluctuations and maintain safe bottomhole circulating temperature (BHCT) across all operations.

Amongst these technologies, modeling of steady-state and transient well thermodynamics provides the foundation for effective downhole temperature management. Early efforts in this field, including the work by Wooley (1980), Marshall & Bentsen, (1982), Ziagos & Blackwell (1986), and Kabir et al. (1996), established the theoretical basis for predicting well temperature evolution in geothermal and high-temperature wells. With advances in numerical methods and computational fluid dynamics (CFD), more comprehensive thermo-hydraulic models have been developed to capture complex drilling operations and formation boundary interactions (Fallah et al., 2019; Ma et al., 2017).

Zhang et al.

Building upon these models, Yang et al. (2019) combined real-time measurements with thermal-hydraulic simulations to quantify the effects of mud properties and operational parameters on BHCT reduction, identifying circulation time and flow rate as key control variables in vertical high-temperature drilling. Wang et al. (2024) further demonstrated a proportional-integral-derivative (PID) controller to automatically reduce BHCT from over 430 °F static temperature to below 290 °F within 5 hours in a ~24,000 ft well. Khaled et al. (2023a, 2023b) proposed a practical downhole heat management strategy that enumerates multiple drilling scenarios and identifies optimal operating parameters for each. More recently, Luu et al. (2024) introduced the concept of MTD, which was later integrated with MPD to form a comprehensive MPD-MTD framework (Duan et al., 2025; van Oort, 2025). This unified approach leverages real-time data, predictive modeling, and automated control to simultaneously regulate BHP and BHCT.

This work extends the control framework introduced in Zhang et al. (2026) by incorporating additional controller schemes and provides a comparative analysis in real-time temperature and pressure management in a deep geothermal test well (Chen et al., 2022, 2024). Three temperature controllers, i.e., PID, linear-quadratic-integral (LQI), and iterative linear-quadratic-regulator (iLQR), are tested using a detailed wellbore thermal-hydraulic model. Through systematic comparison, the study investigates the performance of each controller in terms of response time, control efficiency, and robustness under varying operational conditions. Integrated with an MPD system, the proposed control framework achieves rapid BHCT stabilization and minimal BHP fluctuations.

2 CONTROL-ORIENTED WELL THERMAL MODEL

2.1 Nonlinear Heat Transfer Model

The state-space model developed by Zhang et al. (2026) is adopted in this work for temperature controller design. The drillstring, annulus, and formation is first axially discretized into N segments (Figure 1) with the system control inputs being the surface flow rate Q_{Mud} and flow in temperature T_{in}.

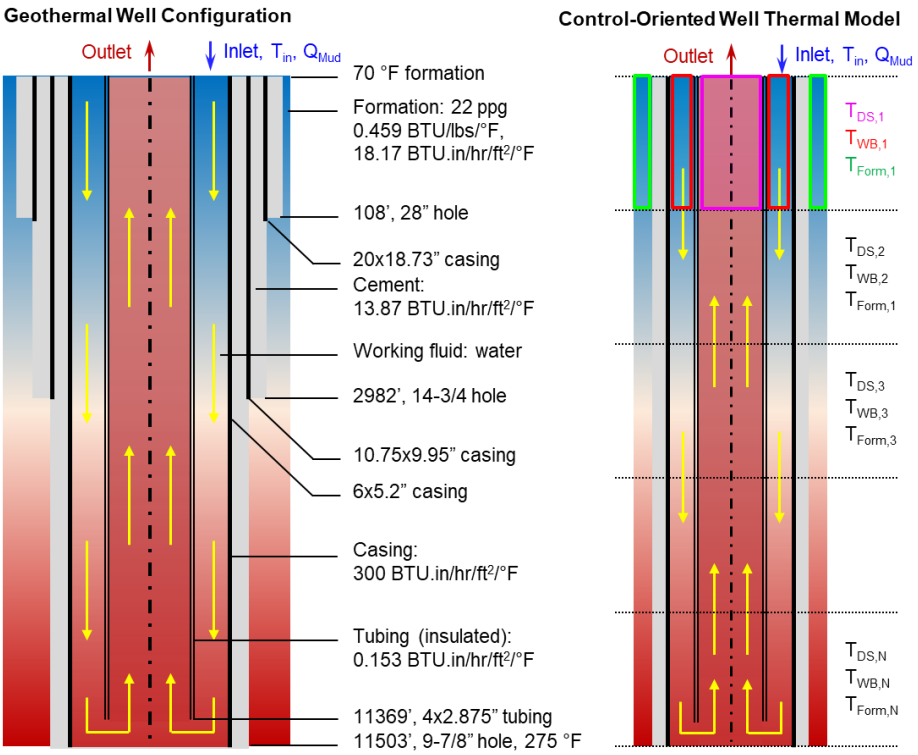


Figure 1—Control-oriented state-space well thermal model. Adapted from Zhang et al. (2026).

The heat transfer between the system states during the reverse circulation can be described as:

$$\rho_{Mud} V_{WB,i} c_{Mud} \dot{T}_{WB,i} = \rho_{Mud} Q_{Mud} c_{Mud} \left(T_{WB,i-1} - T_{WB,i}\right) + \frac{T_{DS,i} - T_{WB,i}}{R_{DS,WB,i}} + \frac{T_{Form,i} - T_{WB,i}}{R_{WB,Form,i}}, i = 2, \dots, N \quad (1)$$

$$\rho_{Mud} V_{DS,i} c_{Mud} \dot{T}_{DS,i} = \rho_{Mud} Q_{Mud} c_{Mud} \left(T_{DS,i+1} - T_{DS,i}\right) + \frac{T_{WB,i} - T_{DS,i}}{R_{DS,WB,i}}, i = 1, \dots, N-1 \quad (2)$$

$$\rho_{Form,i} V_{Form,i} c_{Form,i} \dot{T}_{Form,i} = \frac{T_{WB,i} - T_{Form,i}}{R_{WB,Form,i}} + \frac{T_{FF,i} - T_{Form,i}}{R_{Form,FF,i}}, i = 1, \dots N \quad (3)$$

where ρ_{Mud}, c_{Mud}, and Q_{Mud} denote the mud density, heat capacity, and flow rate; $V_{WB,i}$, $V_{DS,i}$, and $V_{Form,i}$ denote the total volume of the annulus, drillstring, and formation elements; $T_{DS,i}$, $T_{WB,i}$, and $T_{Form,i}$ denote the lumped mud temperature in the drillstring, annulus, and formation at the i^{th} segment of the well; $R_{DS,WB,i}$, $R_{WB,Form,i}$, and $R_{Form,FF,i}$ denote the between drillstring-wellbore, wellbore-formation, and in-formation radial thermal transfer resistance; $T_{FF,i}$ denotes the far-field formation temperature.

The boundary conditions at the surface and the bit are:

$$\rho_{Mud} V_{WB,1} c_{Mud} \dot{T}_{WB,1} = \rho_{Mud} Q_{Mud} c_{Mud} (T_{in} - T_{WB,1}) + \frac{T_{DS,1} - T_{WB,1}}{R_{DS,WB,1}} + \frac{T_{Form,1} - T_{WB,1}}{R_{WB,Form,1}} \quad (4)$$

$$\rho_{Mud} V_{DS,N} c_{Mud} \dot{T}_{DS,N} = \rho_{Mud} Q_{Mud} c_{Mud} (T_{WB,N} - T_{DS,N}) + \frac{T_{WB,N} - T_{DS,N}}{R_{DS,WB,N}} \quad (5)$$

where T_{in} denotes the surface mud temperature into the first element of the annulus. Lumped radial thermal resistances $R_{DS,WB,i}$ and $R_{WB,Form,i}$ are composed of convective and conductive terms and can be further expressed as:

$$R_{DS,WB,i} = \frac{\ln(r_{DS,OD,i}/r_{DS,ID,i})}{2\pi k_{DS,i} L_i} + \frac{1}{2\pi r_{DS,ID,i} h_{DS,ID,i} L_i} + \frac{1}{2\pi r_{DS,OD,i} h_{DS,OD,i} L_i} \quad (6)$$

$$R_{WB,Form,i} = \frac{\ln(r_{Casing,OD,i}/r_{Casing,ID,i})}{2\pi k_{Casing,i} L_i} + \frac{\ln(r_{Cement,OD,i}/r_{Cement,ID,i})}{2\pi k_{Cement,i} L_i} \frac{1}{2\pi r_{WB,ID,i} h_{WB,ID,i} L_i} \quad (7)$$

where $r_{DS,OD,i}/r_{DS,ID,i}$, $r_{WB,OD,i}/r_{WB,ID,i}$, $r_{Casing,OD,i}/r_{Casing,ID,i}$, and $r_{Cement,OD,i}/r_{Cement,ID,I}$ denote the outer/inner radius of drillstring, annulus, casing, and cement at the i^{th} well segment; $k_{DS,i}$, $k_{Casing,i}$, and $k_{Cement,i}$ denote the heat conductivity of drillstring, casing, and cement; L_i denotes the length of i^{th} well segment along the direction of the well center and is unified for all radial elements at the same depth; $h_{DS,ID,i}$ and $h_{DS,OD,i}$ denote the convective heat transfer coefficients at the inner and outer surface of the drillstring; $h_{WB,ID,i}$ denotes the convective heat transfer coefficients at the inner surface of the wellbore and is equal to $h_{DS,ID,i}$. Correspondingly, the radial heat transfer resistance in the formation can be expressed as:

$$R_{Form,FF,i} = \frac{\ln(r_{Form,ID,i}/r_{Form,OD,i})}{2\pi k_{Form,i} L_i} \quad (8)$$

where $k_{Form,i}$ denotes the formation heat conductivity; $r_{Form,OD,i}/r_{Form,ID,i}$ denote the outer/inner radius of the formation element.

The geometry and thermal properties of the investigated geothermal test well, located in Navasota, Texas, USA, are listed in Table 1. Note that the well is fully cased and does not have an open-hole section. Table 1 - Well configuration and parameters (Chen et al., 2022, 2024).

Parameter		Value
Tubing	ID/OD	2.875/4.0 in
	Thermal Conductivity (Vacuum Insulated)	0.153 BTU.in/hr/ft^2/°F
Casing	Intermediate Casing Depth	2,982 ft
	Intermediate Casing ID/OD	9.95/10.75 in
	Production Casing Depth	11,503 ft
	Production Casing ID/OD	5.2/6.0 in
	Thermal Conductivity	300 BTU.in/hr/ft^2/°F
Cement	Thickness - 108 to 2,982 ft	6.765 in
	Thickness - 2,982 to 11,503 ft	1.9375 in
	Thermal Conductivity	13.87 BTU.in/hr/ft^2/°F
Formation	Density	22 ppg
	Heat Capacity	0.459 BTU/lb/°F
	Thermal Conductivity	18.17 BTU.in/hr/ft^2/°F
Mud	Density	8.33 ppg
	Viscosity	2.92E-5 lbf.s/100ft^2
	Heat Capacity	1.0 BTU/lb/°F
	Thermal Conductivity	7.0 BTU.in/hr/ft^2/°F

2.2 Equilibrium and Linearization

For control design, the nonlinear well thermal model needs to be linearized near the equilibrium operation or any system states. For continuous control, the dynamics regarding infinitesimal changes in states is given by:

$$\delta\dot{T}_{DS,i} \approx \left[\frac{Q_{Mud}}{V_{DS,i}} + \frac{1}{\rho_{Mud}V_{DS,i}c_{Mud}R_{WB,DS,i}}\right](\delta T_{DS,i+1} - \delta T_{DS,i}) + \left[\frac{T_{DS,i+1} - T_{DS,i}}{V_{DS,i}} + \frac{T_{WB,i} - T_{DS,i}}{\rho_{Mud}V_{DS,i}c_{Mud}R_{WB,DS,i}^2}\frac{\partial R_{WB,DS,i}}{\partial Q_{Mud}}\right]\delta Q_{Mud} \quad (9)$$

$$\dot{T}_{WB,i} \approx \left[\frac{Q_{Mud}}{V_{WB,i}} + \frac{1}{\rho_{Mud}V_{WB,i}c_{Mud}R_{WB,DS,i}}\right](\delta T_{WB,i-1} - \delta T_{WB,i}) + \frac{\delta T_{Form,i}}{\rho_{Mud}V_{WB,i}c_{Mud}R_{Form,FF,i}} + \left[\frac{T_{WB,i-1} - T_{WB,i}}{V_{WB,i}} + \frac{T_{DS,i} - T_{WB,i}}{\rho_{Mud}V_{WB,i}c_{Mud}R_{WB,DS,i}^2}\frac{\partial R_{WB,DS,i}}{\partial Q_{Mud}} + \frac{T_{Form,i} - T_{WB,i}}{\rho_{Mud}V_{WB,i}c_{Mud}R_{WB,Form,i}^2}\frac{\partial R_{WB,Form,i}}{\partial Q_{Mud}}\right]\delta Q_{Mud} \quad (10)$$

$$\dot{T}_{Form,i} \approx \frac{\delta T_{WB,i} - \delta T_{Form,i}}{\rho_{Mud}V_{Form,i}c_{Mud}R_{WB,Form,i}} - \frac{\delta T_{Form,i}}{\rho_{Mud}V_{Form,i}c_{Mud}R_{Form,FF,i}} + \frac{T_{WB,i} - T_{Form,i}}{\rho_{Mud}V_{Form,i}c_{Mud}R_{WB,Form,i}^2}\frac{\partial R_{WB,Form,i}}{\partial Q_{Mud}}\delta Q_{Mud} \quad (11)$$

Note that thermal resistances between drillstring, annulus, and formation are complex functions of flow rate Q_{Mud} and involves laminar/turbulent flow regimes; their derivatives are therefore calculated numerically. At the surface and bit boundary, linearization of the system is as follows:

$$\dot{T}_{WB,1} \approx \left[\frac{Q_{Mud}}{V_{WB,1}} + \frac{1}{\rho_{Mud}V_{WB,1}c_{Mud}R_{WB,DS,1}}\right](\delta T_{in} - \delta T_{WB,i}) + \frac{\delta T_{Form,1}}{\rho_{Mud}V_{WB,1}c_{Mud}R_{Form,FF,1}} + \left[\frac{T_{WB,in} - T_{WB,1}}{V_{WB,1}} + \frac{T_{DS,1} - T_{WB,1}}{\rho_{Mud}V_{WB,1}c_{Mud}R_{WB,DS,1}^2}\frac{\partial R_{WB,DS,1}}{\partial Q_{Mud}} + \frac{T_{Form,1} - T_{WB,1}}{\rho_{Mud}V_{WB,1}c_{Mud}R_{WB,Form,1}^2}\frac{\partial R_{WB,Form,1}}{\partial Q_{Mud}}\right]\delta Q_{Mud} \quad (12)$$

$$\delta\dot{T}_{DS,N} \approx \left[\frac{Q_{Mud}}{V_{DS,N}} + \frac{1}{\rho_{Mud}V_{DS,N}c_{Mud}R_{WB,DS,N}}\right](\delta T_{WB,N} - \delta T_{DS,N}) + \left[\frac{T_{WB,N} - T_{DS,N}}{V_{DS,N}} + \frac{T_{WB,N} - T_{DS,N}}{\rho_{Mud}V_{DS,N}c_{Mud}R_{WB,DS,N}^2}\frac{\partial R_{WB,DS,N}}{\partial Q_{Mud}}\right]\delta Q_{Mud} \quad (13)$$

It can be observed that the system thermodynamics is linear with regard to the input T_{in} if the input Q_{Mud} is maintained constant. However, changes in Q_{Mud} nonlinearly affect the thermal resistance and heat transportation dynamics in the system. In actual design or operation, continuous system dynamics and control design need to be digitalized for optimal control performance.

In terms of temperature control design, the primary goal is to stabilize the BHCT ($T_{DS,N}$ and/or $T_{WB,N}$) using both T_{in} and Q_{Mud} (classified as multi-input-single-output (MISO) control design). As different T_{in}-Q_{Mud} combinations can map to the same BHCT at steady state, the equilibrium state T_{in}-Q_{Mud}-BHCT relation can be first determined by eliminating the rate of state changes in Eqs. (9) to (13). The equilibrium system BHCT are plotted in Figure 2 for T_{in} between 70 °F and 150 °F and Q_{Mud} between 50 gpm and 400 gpm.

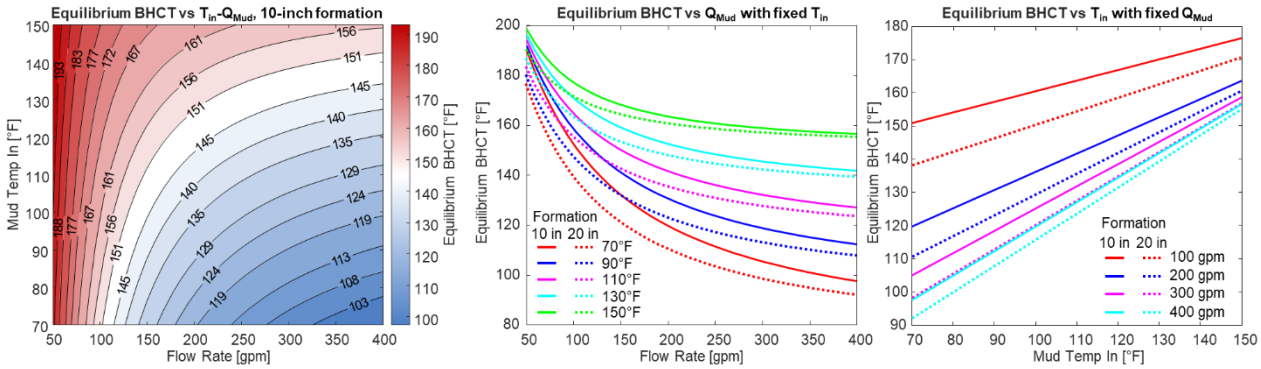


Figure 2—Equilibrium state T_{in}-Q_{Mud}-BHCT relation for 10-/20-inch radial formation thickness.

3 TEMPERATURE CONTROLLER DESIGN

3.1 PID Controllers

As discussed in the previous section, T_{in}-BHCT dynamics is linear with a constant Q_{Mud} input. A T_{in} PI controller (Figure 3) can therefore be designed with the following feedback:

$$T_{in} = P_T\left(T_{BHCT} - T_{BHCT,Ref}\right) + I_T \int \left(T_{BHCT} - T_{BHCT,Ref}\right)dt \tag{14}$$

where P_T and I_T denote the proportional and integral parameters of the controller and need to be tuned based on flow rate; T_{BHCT} and $T_{BHCT,Ref}$ denote the measured/observed BHCT and its reference value. The controller design goal is to achieve the fastest BHCT stabilization time and minimal overshoot with a smooth T_{in}.

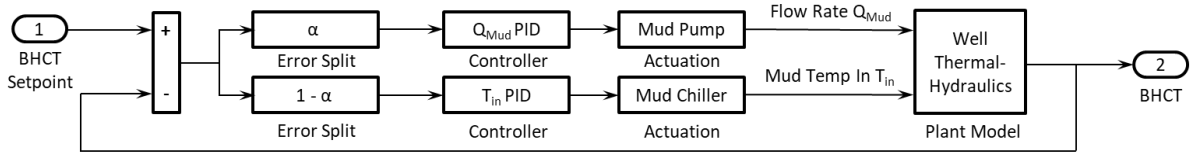


Figure 3—Diagram of the BHCT PID controller.

In comparison to T_{in} PI controllers, Q_{Mud} PI controllers cannot be easily designed as the system dynamics becomes nonlinear:

$$Q_{Mud} = P_Q\left(T_{BHCT} - T_{BHCT,Ref}\right) + I_Q \int \left(T_{BHCT} - T_{BHCT,Ref}\right)dt \tag{15}$$

Using a single set of PID parameters for Q_{Mud} control can result in suboptimal or even diverging BHCT responses. Gain scheduling or other nonlinear control methods can be incorporated for robust Q_{Mud} control. The T_{in} and Q_{Mud} PID controllers can be combined as a T_{in}-Q_{Mud} PID controller, using an error split factor α:

$$\begin{cases} T_{in} = (1-\alpha)P_T\left(T_{BHCT} - T_{BHCT,Ref}\right) + (1-\alpha)I_T \int \left(T_{BHCT} - T_{BHCT,Ref}\right)dt \\ Q_{Mud} = \alpha\, P_Q\left(T_{BHCT} - T_{BHCT,Ref}\right) + \alpha\, I_Q \int \left(T_{BHCT} - T_{BHCT,Ref}\right)dt \end{cases} \tag{16}$$

3.2 LQI Controllers

With the state-space well heat transfer model, LQI controllers can also be developed for BHCT control. In an LQI framework, an augmented system is constructed by adding an integral state that represents the accumulated tracking error between the system output and its reference (Figure 4).

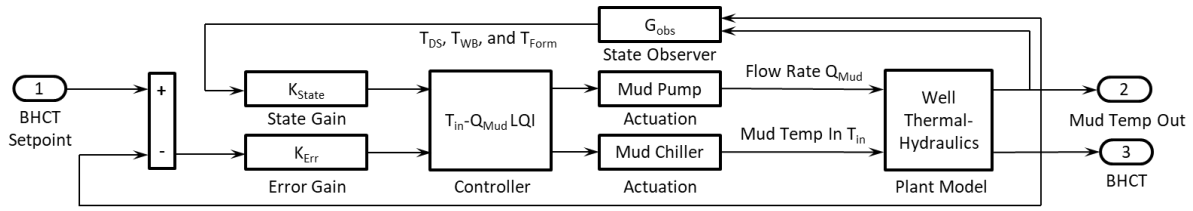


Figure 4—Diagram of the BHCT LQI controller.

More specifically, the LQI controller is developed based on the linear model at a nominal T_{in}.= 70 °F and Q_{Mud} = 300 gpm. The design of BHCT LQI controller can be described as the following optimization problem:

$$\min_{K_{State},K_{Err}} J = x_T^T Q_T x_T + \sum_{t=0}^{T-1}\left(x_t^T Q_t x_t + R_T T_{in,t}^2 + R_Q Q_{Mud,t}^2\right) \tag{17}$$

$$x_t = \left[T_{DS,i}, T_{WB,i}, T_{Form,i}, Err_{BHCT}\right]_t^T, i = 1,2,\dots N, t = 1,2,\dots,T \tag{18}$$

$$u_t = [K_{State} \quad K_{Err}]x_t = [T_{in}, Q_{Mud}]_t, t = 1,2,\dots,T-1 \tag{19}$$

$$Err_{BHCT,t} = \sum_{k=0}^{t}\left(T_{BHCT,k} - T_{BHCT,Ref,k}\right), t = 1,2,\dots,T \tag{20}$$

$$Q_t = \left[\left[Q_{DS,i}, Q_{WB,i}, Q_{Form,i}\right], Q_{Err}\right]_t, i = 1,2,\dots N, t = 1,2,\dots,T \tag{21}$$

where x_t denotes the stacked system states at time t; Q_t, R_T and R_Q denote cost weight on the second order state and input deviation; J denotes the cost function to be optimized; K_{State} and K_{Err} denote the static state and error

gains to be optimized; Err_{BHCT} denotes the integrated error of BHCT; Q_{DS}, Q_{WB}, Q_{Form}, and Q_{Err} denote the weight on T_{DS}, T_{WB}, T_{Form}, and Err_{BHCT}, respectively.

Overall, compared to PID controllers, LQI controllers offer a more robust and straightforward solution for BHCT regulation under nominal conditions. It assumes a linear time-invariant system and may lose accuracy when applied to highly nonlinear or time-varying well thermodynamics. The tuning of the weighting matrices also requires experience and may not guarantee consistent performance across different operating conditions.

3.3 iLQR Controllers

Considering the large nonlinearity of well thermodynamics and the dual-impact of T_{in} and Q_{Mud} on BHCT, an iLQR controller can also be designed for BHCT management. Instead of relying on fixed linearized dynamics, iLQR iteratively linearizes the nonlinear well thermal model around the current state (Figure 5).

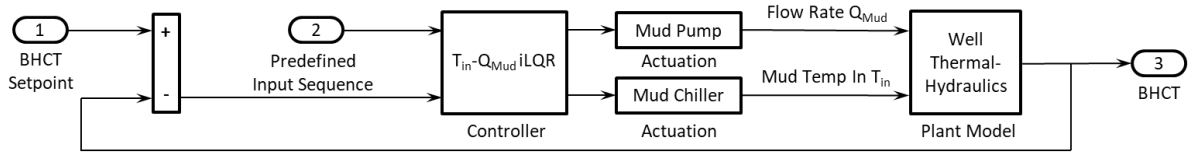


Figure 5—Diagram of the BHCT iLQR controller.

In the iLQR control framework, the reference BHCT and the desired steady-state T_{in} and Q_{Mud} inputs can be more flexibly tracked. More specifically, nonlinear system dynamics Eqs. (1) to (8) are first discretized in time domain and then tracked strictly given a T_{in} and Q_{Mud} input sequence. The cost function to be minimized for the control horizon is:

$$\min_{T_{in},Q_{Mud}} J = \tilde{x}_T^T Q_T \tilde{x}_T + \sum_{t=0}^{T-1} \left(\tilde{x}_t^T Q_t \tilde{x}_t + R_{Q,t} \tilde{Q}_{Mud,t}^2 + R_{T,t} \tilde{T}_{in,t}^2 \right) \tag{22}$$

$$x_t = \left[T_{DS,i}, T_{WB,i}, T_{Form,i} \right]_t^T, i = 1,2, \dots N, t = 1,2, \dots, T \tag{23}$$

$$\tilde{x}_t = \left[T_{DS,i} - \overline{T}_{DS,i}, T_{WB,i} - \overline{T}_{WB,i}, T_{Form,i} - \overline{T}_{Form,i} \right]_t^T = x_t - \bar{x}_t, i = 1,2, \dots N, t = 1,2, \dots, T \tag{24}$$

$$\tilde{Q}_{Mud,t} = Q_{Mud,t} - \overline{Q}_{Mud,t}, t = 1,2, \dots, T-1 \tag{25}$$

$$\tilde{T}_{in,t} = T_{in,t} - \overline{T}_{in,t}, t = 1,2, \dots, T-1 \tag{26}$$

$$Q_t = \left[Q_{DS,i}, Q_{WB,i}, Q_{Form,i} \right]_t, i = 1,2, \dots N, t = 1,2, \dots, T \tag{27}$$

where $\bar{x}_t$, $\overline{Q}_{Mud,t}$, and $\overline{T}_{in,t}$ denote the predefined system dynamics and input trajectories. Essentially, solving the iLQR problem generates a sequence of T_{in} and Q_{Mud} inputs that minimize the deviation of the system dynamics from the predetermined $\bar{x}_t$, measured by the cost function J.

It is important to note that the iLQR controller relies on accurate system models and local linearization around the nominal trajectory. When model mismatch or unmodeled nonlinearities are significant, the controller's predicted trajectory may diverge from the true system behavior, leading to suboptimal or unstable performance.

3.4 Integration with MPD

Theoretically, the implementation of the proposed BHCT controllers faces several practical limitations and challenges:

1. Mud chiller performance: The cooling capacity of surface mud chillers can be insufficient to achieve the desired inlet temperature reduction, particularly at high circulation rates or in deep, high-temperature, high-angle wells.
2. Pump operation constraints: The available mud pumps may have limited controllability or restricted operational ranges. Variations in flow rate are often constrained by hole cleaning, equivalent circulating density (ECD) limits, MPD system requirements, and rig equipment capacity.
3. Thermal-hydraulic coupling: Downhole temperature changes affect drilling mud density, viscosity, and pressure, which in turn affects the well hydraulics. These coupled nonlinear effects complicate the well's thermal-hydraulic behavior and challenges the robustness of well temperature control systems.

To address these limitations, it is recommended that the proposed BHCT controllers, or more broadly, MTD technologies, be integrated with MPD systems to enable comprehensive well pressure-temperature control (Figure 6).

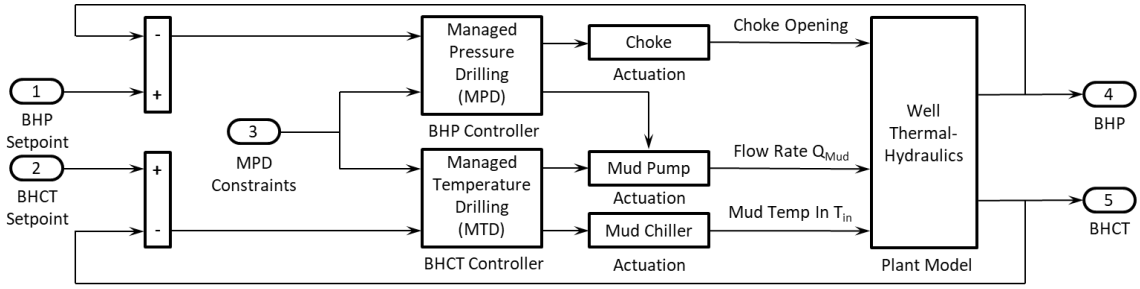


Figure 6—Diagram of the integrated BHP and BHCT control (MPD-MTD setup).

The coupling between the MPD and MTD systems is bidirectional. On one hand, operational constraints imposed by the MPD system (e.g., allowable flow-rate and maximum pump ramp rate) define the feasible control space for the MTD system. On the other hand, slow thermal effects (e.g., formation cooling and fluid property changes) introduce pressure drifts that are compensated in real time by the fast-reacting MPD control loop. In this way, the MPD-MTD integration enables a hierarchical multi-time-scale control strategy, where MPD manages the fast hydraulics and MTD regulates the slower thermal transients.

4 CONTROLLER PERFORMANCE

4.1 Simulation Results

To evaluate the effectiveness and efficiency of the developed BHCT controllers, the well circulation is simulated with reference BHCT values of 130, 150, and 170 °F, each maintained for 100 min. The simulation starts from a static well temperature profile, where the mud and formation temperatures are equal to the far-field temperature at all depths. The well configuration listed in Table 1 is adopted for the BHCT PID, LQI, and iLQR controllers. The control inputs are limited to 70-150 °F for T_{in} and 30-400 gpm for Q_{Mud}.

Figure 7 illustrates close-loop well thermal responses under different BHCT PID controllers. It can be observed that the T_{in} PID controller saturates at 150 °F when attempting to reach a 170 °F BHCT with 300 gpm (see also Figure 2) and exhibits a BHCT dead zone of approximately 10 min due to mud transportation delay. For the Q_{Mud} and T_{in}-Q_{Mud} PID controllers, zero BHCT steady state errors are achieved for all three 100-min stages without saturation. Specifically, with a constant 70 °F T_{in}, the Q_{Mud} PID controller reaches BHCT targets of 130, 150, and 170 °F with input flow rate of 156, 105, and 72 gpm, respectively. When both T_{in} and Q_{Mud} are controlled, the T_{in}-Q_{Mud} PID controller achieves the BHCT setpoints with (74 °F, 173 gpm), (86 °F, 117 gpm), and (92 °F, 81 gpm), respectively. Modification of these equilibrium state T_{in}-Q_{Mud} can be achieved through adjusting the error split between the two inputs in the T_{in}-Q_{Mud} PID controller, incorporating a feedforward term, or a re-design of the controller based on real-time system equilibrium. The adopted PID controller parameters in Figure 7 are: P_T = 0.64, I_T = 0.001269 sec^{-1}, P_Q = -10.60 gpm $°F^{-1}$, I_Q = -0.00542 gpm $°F^{-1}$ sec^{-1}, and α = 0.8.

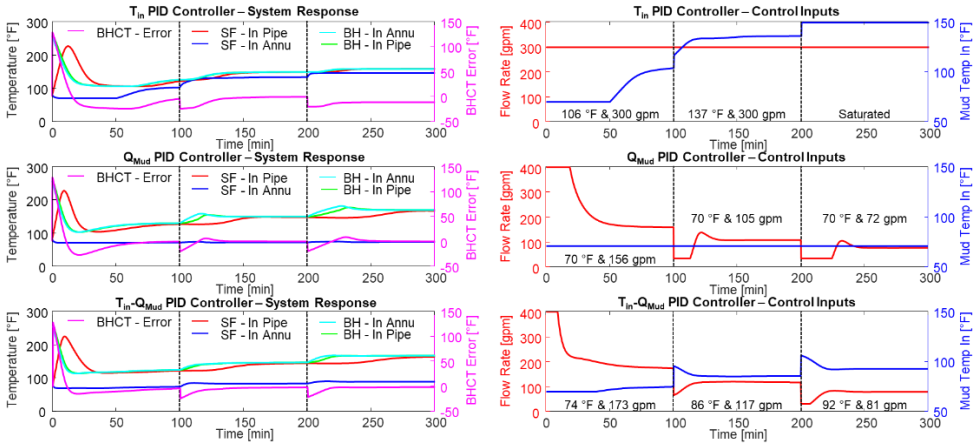


Figure 7—BHCT PID Controllers. Left: Close-loop system dynamics with reference BHCT equal to 130, 150, and 170 °F. Right: Corresponding T_{in} and Q_{Mud} inputs for the BHCT control.

Similarly, the BHCT LQI controllers, using T_{in}-only, Q_{Mud}-only, and T_{in}-Q_{Mud} inputs, are simulated under the same constraints, BHCT references, and initial conditions. As shown in Figure 8, the steady-state inputs of the T_{in} and Q_{Mud} LQI controllers matches those from the PID controllers since each represents a one-to-one input-output relationship when the other variable is held constant. Meanwhile, T_{in}-Q_{Mud} LQI controller reaches the 130, 150,

and 170 °F BHCT setpoints at the three stages with (80 °F, 177 gpm), (100 °F, 133 gpm), and (118 °F, 93 gpm), respectively. Compared to the BHCT PID controllers, the LQI controllers are faster, more robust, and more efficient. However, as linear controllers, their closed-loop performance still diverges from the designed behavior when operating far from the nominal linearization point. The adopted LQI controller parameters are: R_T = 1 °F^{-2}, R_Q = 0.08 gpm^{-2}, Q_{DS} = Q_{WB}= Q_{Form} = 10 °F^{-2}, Q_{Err} = 0.002 °F^{-2} sec^{-2}.

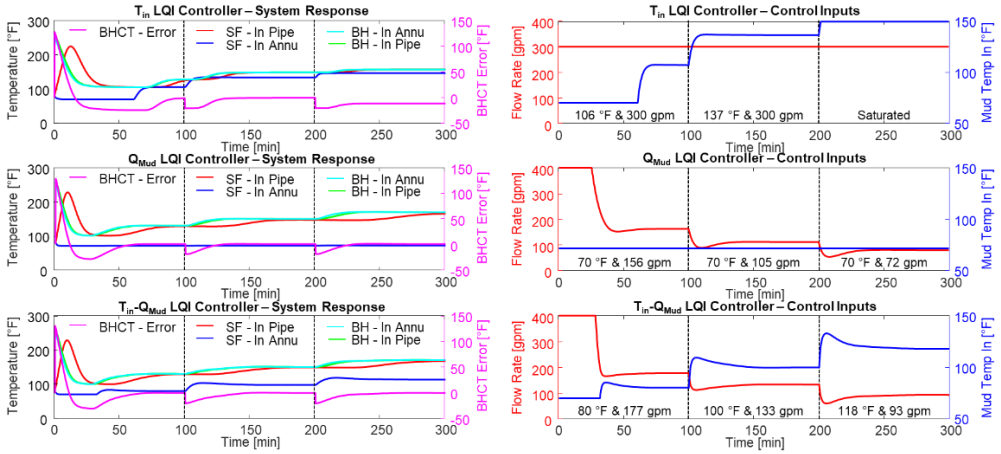


Figure 8—BHCT LQI Controllers. Left: Close-loop system dynamics with reference BHCT equal to 130, 150, and 170 °F. Right: Corresponding T_{in} and Q_{Mud} inputs for the BHCT control.

In comparison to the PID and LQI controllers, the iLQR controller is designed for nonlinear systems and performs feasible trajectory optimization over the entire control horizon. Based on Figure 2, multiple T_{in}-Q_{Mud} combinations can achieve the steady-state BHCTs of 130, 150, and 170 °F. Different field constraints, such as hole cleaning, surface equipment capacity and well control can be considered to determine T_{in} and Q_{Mud}. For example, one can increase BHCT from 130 °F to 150 °F and 170 ° following the inputs path of (100 °F, 250 gpm), (118 °F, 170 gpm), and (127 °F, 100 gpm) (middle row of Figure 9), which naturally decreases the Q_{Mud} setpoint while increasing T_{in}. The same BHCT increment can be achieved with (107 °F, 300 gpm), (89 °F, 120 gpm), and (80 °F, 75 gpm) (bottom row of Figure 9), which decreases T_{in} and Q_{Mud} at the same time. For iLQR controllers simulated in Figure 9, the maximum rate of change of T_{in} and Q_{Mud} input are limited to 5 °F min^{-1} and 30 gpm min^{-1}. With these added constraints, iLQR controllers still provide greater flexibility, smoother input transitions, and overall better tracking of the reference than PID and LQI controllers. The tuned iLQR penalization coefficients are R_T = 1 °F^{-2}, R_Q = 0.2 gpm^{-2}, Q_{DS} = Q_{WB}= Q_{Form} = 8 °F^{-2}.

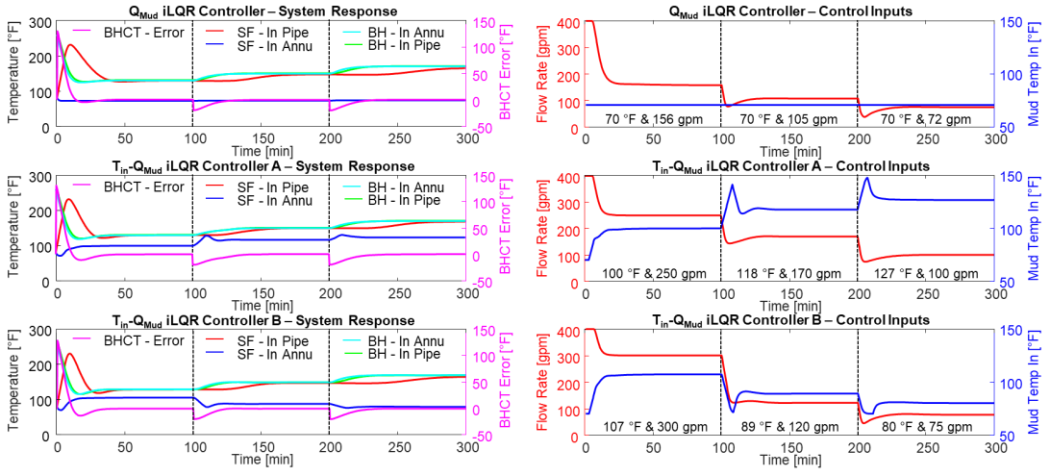


Figure 9—BHCT iLQR Controllers with T_{in} and Q_{Mud} slope limiter. Left: Close-loop system dynamics with reference BHCT equal to 130, 150, and 170 °F. Right: Corresponding T_{in} and Q_{Mud} inputs for the BHCT control.

4.2 Comparison between Controllers

Table 2 quantitatively summarizes the simulated controller performance shown in Figure 7 through Figure 9. The results highlight the relative response speed, control feasibility, and input utilization characteristics of each control strategy.

Table 2 - Controller design and performance summary.

Controller		1st Stage: Ref BHCT = 130 °F			2nd Stage: Ref BHCT = 150 °F			3rd Stage: Ref BHCT = 170 °F		
Design	Input	1 °F Error [min]	T_{in} [°F]	Q_{Mud} [gpm]	1 °F Error [min]	T_{in} [°F]	Q_{Mud} [gpm]	1 °F Error [min]	T_{in} [°F]	Q_{Mud} [gpm]
PID	T_{in}	>100	106	300	73	137	300	Saturated	Saturated	Saturated
	Q_{Mud}	>100	70	156	62	70	105	78	70	72
	T_{in}-Q_{Mud}	>100	74	173	84	86	117	52	92	81
LQI	T_{in}	>100	106	300	43	137	300	Saturated	Saturated	Saturated
	Q_{Mud}	60	70	156	27	70	105	27	70	72
	T_{in}-Q_{Mud}	64	80	177	42	100	133	48	118	93
iLQR	Q_{Mud}	33	70	156	35	70	105	32	70	72
	T_{in}-Q_{Mud} A	40	100	250	39	118	170	38	127	100
	T_{in}-Q_{Mud} B	35	107	300	23	89	120	31	80	75

It can be observed that in the 1st stage, the BHCT stabilization time is longer than in the subsequent stages because the well initially starts from static temperature conditions. Once the wellbore is thermally stabilized and the circulation reaches a quasi-steady state, the system dynamics become faster, enabling quicker convergence to the 150 °F and 170 °F BHCT setpoints in the 2nd and 3rd stages. In general, the LQI controllers provide moderate improvement over PID controllers, with faster response and better consistency. The Q_{Mud} and T_{in}-Q_{Mud} LQI controllers achieve a 1 °F BHCT settling time of 27-64 min. In contrast, iLQR controllers demonstrate the best overall performance. The Q_{Mud} iLQR controller achieves 1 °F BHCT settling time of 32-35 min, which is nearly 2x faster than the linear Q_{Mud} controllers in some scenarios. The T_{in}-Q_{Mud} iLQR controllers can achieve 1 °F BHCT settling within 23-40 min across all BHCT levels.

5 CONCLUSION

This study presents a novel temperature-pressure management framework for geothermal and HPHT wells. The proposed solution is composed of a control-oriented well thermal model, multiple BHCT control strategies (PID, LQI, and iLQR), and an MTD-MPD system for proactive real-time control of mud flow rate, inlet mud temperature, and choke opening. Thermal-hydraulics simulations in a 11,503 ft geothermal test well demonstrates that the system can rapidly stabilize BHCT within 40 minutes while maintaining BHP fluctuations within 30 psi.

Among the tested controllers, the iLQR-based scheme achieved the fastest settling time and highest robustness, followed by the LQI controller, which provided smoother transitions and reduced overshoot. The PID controller offered stable but slower convergence, serving as a useful baseline for comparison. Compared to conventional open-loop control methods, the integrated MTD-MPD framework enables rapid, automated suppression of thermal-pressure shocks, with associated protection of downhole equipment and wellbore integrity, and offers significant improvement potential for geothermal drilling efficiency and energy recovery.

REFERENCES

Chen, G., Wright, C., & Goswami, J. C. (2022, June 26). Wellbore Shut-In Temperature Study After Fluid Circulations in a Fit-For-Purpose Research Well in Grimes County, Texas. 56th U.S. Rock Mechanics/Geomechanics Symposium.

Chen, G., Wright, C., Liu, J., Gomez, C., & Garcia, A. (2024, June 23). Modeling a Deep Coaxial Closed-Loop Vacuum Insulated Tubing (VIT) Completion in a Geothermal Research Test Well Using FEFLOW. 58th U.S. Rock Mechanics/Geomechanics Symposium.

Duan, X., Zhang, Y., Ashok, P., Chen, D., & van Oort, E. (2025). Integration of MPD with Managed Temperature Drilling (MTD) for Geothermal and HPHT Drilling. IADC/SPE Managed Pressure Drilling & Underbalanced Operations Conference & Exhibition.

Fallah, A., Gu, Q., Ma, Z., Karimi Vajargah, A., Chen, D., Ashok, P., van Oort, E., & May, R. (2019). An Integrated Thermal and Multi-Phase Flow Model for Estimating Transient Temperature Dynamics During Drilling Operations. SPE/IADC International Drilling Conference and Exhibition.

Kabir, C. S., Hasan, A. R., Kouba, G. E., & Ameen, M. M. (1996). Determining Circulating Fluid Temperature in Drilling, Workover, and Well Control Operations. SPE Drilling & Completion, 11(02), 74-79.

Khaled, M. S., Chen, D., Ashok, P., & van Oort, E. (2023). Drilling Heat Maps for Active Temperature Management in Geothermal Wells. SPE Journal, 28(04), 1577-1593.

Khaled, M. S., Wang, N., Ashok, P., & van Oort, E. (2023). Downhole heat management for drilling shallow and ultra-deep high enthalpy geothermal wells. Geothermics, 107, 102604.

Luu, A., Wang, N., Gu, Q., Khaled, M., Ashok, P., Chen, D., & van Oort, E. (2024). Managed Temperature Drilling: An Automated Real-Time Controller for Downhole Temperature Control in Geothermal and HPHT Wells. IADC/SPE International Drilling Conference and Exhibition.

Ma, Z., Karimi, A., Ambrus, A., Ashok, P., Chen, D., & van Oort, E. (2017). A Comprehensive Hydraulic Software Package for Drilling Operations. AADE National Technical Conference and Exhibition.

Marshall, D. W., & Bentsen, R. G. (1982). A Computer Model to Determine the Temperature Distributions In a Wellbore. Journal of Canadian Petroleum Technology, 21(01).

van Oort, E. (2025). Managed Pressure Drilling: Fundamentals, Methods and Applications. Elsevier.

Wang, C., Liu, H., Yu, G.-W., Yu, C., Liu, X.-M., & Huang, P. (2024). Wellbore-heat-transfer-model-based optimization and control for cooling downhole drilling fluid. Petroleum Science, 21(3), 1955-1968.

Wooley, G. R. (1980). Computing Downhole Temperatures in Circulation, Injection, and Production Wells. Journal of Petroleum Technology, 32(09), 1509-1522.

Yang, M., Luo, D., Chen, Y., Li, G., Tang, D., & Meng, Y. (2019). Establishing a practical method to accurately determine and manage wellbore thermal behavior in high-temperature drilling. Applied Energy, 238, 1471-1483.

Zhang, Y., Duan, X., Callerio, S., Ashok, P., Chen, D., van Oort, E., Chen, G., Wright, C., Garcia, A. (2026). Automation of Simultaneous Temperature and Pressure Control in a Geothermal Test Well. SPE/IADC International Drilling Conference and Exhibition.

Ziagos, J. P., & Blackwell, D. D. (1986). A model for the transient temperature effects of horizontal fluid flow in geothermal systems. Journal of Volcanology and Geothermal Research, 27(3-4), 371-397.